High Resolution Quantitative Susceptibility Mapping at 9.4T

A. Deistung[1], J. Budde[2], F. Schweser[1], J. Hoffmann[2], R. Pohmann[2], and J. R. Reichenbach[1]

[1]Medical Physics Group, Department of Diagnostic and Interventional Radiology I, Jena University Hospital, Jena, Germany, [2]Max Planck Institute for Biological Cybernetics, Tübingen, Germany

INTRODUCTION

Susceptibility weighted imaging at ultrahigh magnetic fields ($B_0 \geq 7T$) has become a new forefront of research, triggered by the anticipated increase in signal-to-noise ratio (SNR), higher spatial resolution, and improved contrast mechanisms. Employing these advantages superb anatomical contrast has already been demonstrated for both magnitude [1,2] and phase images [2-4]. These phase images represent the basis for a promising technique, referred to as quantitative magnetic susceptibility mapping (QSM), which has recently been introduced to provide a novel quantitative and local anatomical contrast. However, image reconstruction from multi-channel data becomes complicated at these field strengths since volume body coils are generally not available [5], which are usually required for mapping the spatial sensitivities of the coil array. To this end, Hammond et al. [6] suggested combining multi-channel phase images by taking into account the channel-dependent phase offset estimated from the single coil images within the same homogenous region of interest. Application of this reconstruction method at field strengths exceeding 7T is, however, hampered due to extremely localized B_1 coil sensitivities. Therefore, this contribution presents a new reconstruction technique for combining multi-channel phase images based on a dual-echo GRE acquisition. The method is applied to multi-channel GRE data acquired at 9.4 T with 0.4 mm isotropic spatial resolution, and state-of-the-art post-processing is performed, including QSM.

MATERIAL AND METHODS

Data Acquisition: High-resolution brain data of a healthy volunteer was acquired with a 3 D dual-echo gradient-echo sequence ($TE_1/TE_2/TR/FA$ =12.1ms/25.5ms/34ms/15°) on a 9.4T MRI system (9.4T Magnetom, Siemens Medical Solutions, Germany) using a custom-built elliptical 16-channel transmit/receive array head coil. B_1-shimming was conducted as described by Hoffmann et al. [7]. Data was acquired with an isotropic voxel size of 0.4 mm covering a field of view of $172 \times 229 \times 35.2$ mm^3 (partial Fourier 7/8 and 6/8 along phase and slice encoding direction).

$$\varphi_{k,0} = \varphi_{k,1} - \left(\frac{\varphi_{k,2} - \varphi_{k,1}}{TE_2 - TE_1}\right) \cdot TE_1 \qquad (1)$$

$$\varphi_{c,e} = \arg\left(\sum_{k=1}^{n} W_k \cdot S_k \cdot e^{j \cdot (\varphi_{k,e} - \varphi_{k,0})}\right) \qquad (2)$$

$$S_k = P\left\{\frac{m_{k,1}}{m_{SoS,1}}\right\} \qquad (3)$$

Data Processing: The combination of multi-channel magnitude $m_{SoS,e}$ and phase $\varphi_{c,e}$ data was performed for each echo e individually. Magnitude images were reconstructed by the sum-of-squares (SoS) method [8]. To combine the phase data, the phase offset $\varphi_{k,0}$ of each channel k was calculated by the linear estimation in Eq. 1, where $\varphi_{k,1}$ and $\varphi_{k,2}$ are the unwrapped phase values of channel k at echo times TE_1 and TE_2, respectively [9]. For each echo e, the combined phase image, $\varphi_{c,e}$, was then calculated by taking the arc tangent of the complex summation over all channels k, as shown in Eq. 2. The binary mask W_k identifies regions with sufficiently high SNR. S_k is an estimate for the sensitivity of coil element k, which was calculated by 5th order polynomial fitting to the ratio of channel k's magnitude $m_{k,1}$ and SoS-reconstructed magnitude according to Eq. 3. The operator P{} denotes polynomial fitting. Phase aliasing was resolved by 3D phase unwrapping [10] and background phase contributions were eliminated with the SHARP technique [11] and scaled by $-2\pi \cdot TE$ to yield frequency maps showing the Larmor frequency variation in Hz. Finally, susceptibility maps from background-corrected phase images were computed with an algorithm described by Schweser et al. [12].

RESULTS

Figure 1 presents slices (gap between slices of 1.2 mm) of frequency and susceptibility images showing sections of the cerebral cortex of the occipital and temporal lobe. The non-local magnetic field contributions (Fig. 1a,c,e) were successful converted into a local map of magnetic susceptibility (Fig. 1b,d,f). This is indicated by the compensation of external frequency contributions in the vicinity of venous vessels (see black arrows). Susceptibility maps varied across the cortical thickness, suggesting a layer-specific contrast (see red arrow in Fig. 1b). Interestingly, layer-specific contrast of this corresponding cortex structure is barely visible in the frequency map (see red arrow in Fig. 1a). The magnetic susceptibility of gray matter also varies depending on the cortical region as indicated by the green arrows in Fig. 1d.

DISCUSSION

We have presented a new approach to combine multi-channel phase images by estimating the channel independent coil offset from a dual-echo approach. The method was successfully applied to reveal the cortical architecture using SHARP and QSM. If the sequence cannot be acquired with multiple echoes, an additional low resolution double-echo scan may be employed to estimate the coil offsets. Alternatively, the receiver dependent phase offset may be estimated relative to a single reference coil element and, thus, is also suitable for combining single echo data, but it cannot remove the individual offset of the reference coil element. The frequency maps demonstrated excellent contrast between gray and white matter structures. However, the underlying source of the phase contrast between gray and white matter is currently under debate and is suggested to arise from differences in myelin content and structure, or to originate from other susceptibility sources, such as iron and deoxyhemoglobin, or from exchange between free water and macromolecules, or anisotropic microscopic tissue architecture. The susceptibility contrast is, contrary to the phase contrast, local and depicts the underlying anatomy directly. Therefore, intracortical variations could be identified more accurately than in frequency images, suggesting that intracortical contrast is related to magnetic susceptibility. The regional variations in magnetic susceptibility of cortical gray matter between the occipital and temporal lobe may also be attributed to different iron concentrations [13]. Future investigations will involve QSM with more sophisticated algorithms, e.g. using prior information about the susceptibility map [14] or multi-angle acquisitions [11,15] to produce susceptibility maps with reduced artifact level that depict local tissue architecture more clearly. Nevertheless, very high-resolution phase imaging and QSM at ultrahigh-field strengths will certainly help to improve the understanding of a wide range of clinical applications and pathologies.

REFERENCES

[1] Li TQ, et al. *Neuroimage*. 2006;32(3):1032-40.[2] Deistung A, et al. *MagnReson Med*. 2008;60(5):1155-68.[3] Duyn JH. *ProcNatlAcadSci U S A*. 2007;104(28):11796-801.[4] Budde J, et al.*MagnReson Med*. 2001.[5] Ladd ME. *Top MagnReson Imaging*. 2007;18(2):139-52.[6] Hammond KE, et al. *Neuroimage*. 2008; 39(4):1682-92.[7] Hoffmann, J., et al. *Procof ISMRM*.2010:1470.[8] Roemer PB, et al. *MagnReson Med*. 1990. 16(2):192-225.[9] Schweser F, et al. *Proc of German Section of ISMRM*. 2010:5[10] Abdul-Rahman HS, et al. *ApplOpt*. 2007;46(26):6623-3.[11]Schweser F, et al. *Neuroimage*. 2010.[12]Schweser F, et al. Med Phys. 2010;37(9):5165-5178. [13] Hallgren B, Sourander P. *J Neurochem*. 1958;3(1):41-51. [14] de Rochefort L, et al. *MagnReson Med*. 2010;63(1):194-206. [15] Liu T, et al. *MagnReson Med*. 2009;61(1):196-204.
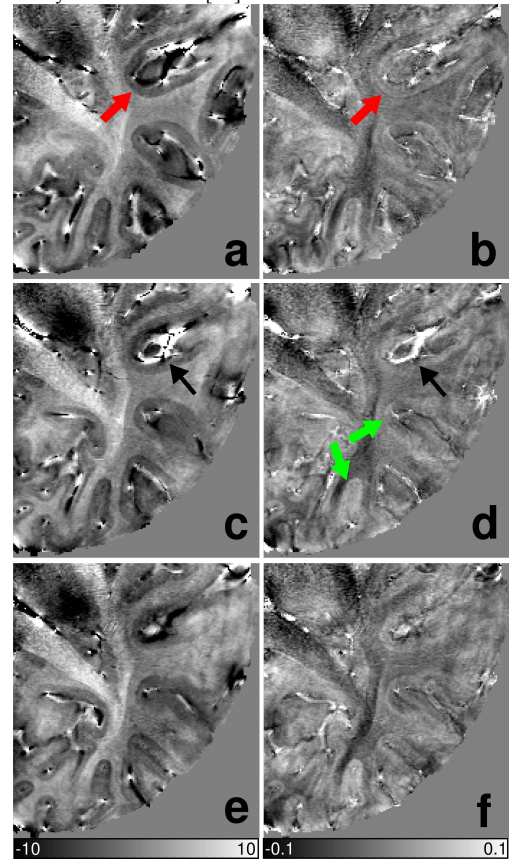
Figure 1: Frequency maps (in Hz) and corresponding susceptibility maps (in ppm) computed from the first echo are shown in the left and right column, respectively. Rows indicate similar slice location. The distance between the presented slices is 1.2 mm, respectively.